THE JOURNAL OF BIOLOGICAL CHEMISTRY VOL. 285, NO. 18, pp. 13816–13826, April 30, 2010

The Contact Region between Three Domains of the Extracellular Loop of ASIC1a Is Critical for Channel Function*[S]

Received for publication, November 19, 2009, and in revised form, February 6, 2010 Published, JBC Papers in Press, March 9, 2010, DOI 10.1074/jbc.M109.086843

Benoît Bargeton and Stephan Kellenberger[1]

From the Department of Pharmacology and Toxicology, University of Lausanne, CH-1005 Lausanne, Switzerland

Acid-sensing ion channels are members of the epithelial Na^+ channel/degenerin family. They are neuronal nonvoltage-gated Na^+ channels that are activated by extracellular acidification. In this study, we investigated the role of a highly conserved region of the extracellular part of ASIC1a that forms the contact between the finger domain, the adjacent β-ball, and the upper palm domain in ASIC1a. The finger domain contributes to the pH-dependent gating and is linked via this contact zone to the rest of the protein. We found that mutation to Cys of residues in this region led to decreased channel expression and current amplitudes. Exposure of the engineered Cys residues to Cd^{2+} or to charged methane thiosulfonate sulfhydryl reagents further reduced current amplitudes. This current inhibition was not due to changes in acid-sensing ion channel pH dependence or unitary conductance and was likely due to a decrease of the probability of channel opening. For some mutants, the effect of sulfhydryl reagents depended on the pH of exposure in the range 7.4 to 6.8, suggesting that this zone undergoes conformational changes during inactivation. Our study identifies a region in ASIC1a whose integrity is required for normal channel function.

Acid-sensing ion channels (ASICs)[2] are neuronal nonvoltage-gated Na^+ channels that are activated by a rapid drop in extracellular pH (1, 2). They are members of the epithelial Na^+ channel/degenerin family of ion channel proteins (3). Functional ASICs are formed by homo- or heterotrimeric assembly of ASIC subunits 1a, 1b, 2a, 2b, and 3. Each subunit has intracellular N and C termini and two transmembrane domains that are separated by a large extracellular loop that makes up ~70% of the protein mass. The crystal structure of chicken ASIC1 shows the complex organization of the extracellular loop (Fig. 1*A*) (4, 5). Expression in nociceptive neurons and activation by protons suggest that ASICs may contribute to pain sensation (6), and evidence for such a role has been provided in several animal pain models (7–9). ASIC1a in the central nervous system plays a role in memory formation (10) and the expression of fear (10, 11). ASIC1a is also an important mediator of cell injury induced by conditions associated with acidosis in the mammalian nervous system (12).

The molecular mechanisms of ASIC activation by extracellular acidification are complex and not completely understood. Several studies suggest that conformational changes contribute to channel opening (5, 13, 14). Although protons are the only ASIC activators identified so far, ASIC activity is known to be modulated by many different mechanisms. A study on ASIC2a showed that Zn^{2+} shifts the pH dependence of activation to less acidic values and that for this effect two His residues are critical, His-162 and His-339 (15). His-162 of ASIC2a corresponds to His-163 in human ASIC1a (hASIC1a) and is conserved in all ASICs but not in other epithelial Na^+ channel/degenerin family members. Analysis of the ASIC structure (4, 5) shows that His-163 is located at a point that connects three structural domains of the ASIC extracellular loop, the finger, the β-ball, and the upper part of the palm. Fig. 1, *A* and *B*, are based on a human ASIC1a homology model derived from the 2QTS chicken ASIC1 structure (see "Experimental Procedures"; stereo views of Fig. 1, *A* and *B* are shown in supplemental Fig. S1) (5). Fig. 1*A* also indicates the names of the different ASIC domains, as they were introduced in the initial ASIC structure paper (5). The palm (*yellow* in Fig. 1*A*) stretches vertically from the membrane up to the knuckle (*turquoise)* along the central vertical axis of the channel and contains a lower β-sheet and an upper β-sheet that interacts with the β-ball (*orange*). The β-ball is a sphere formed by several crossing β-strands and loops and is located at the same distance from the membrane as the upper palm, between the upper palm, the thumb, and the finger. The main part of the finger (Fig. 1*A*, *purple*) consists of residues 100–165 and includes the α-helices α1–α3 and is connected covalently to the rest of the protein in the zone around His-163 that we name in this study "finger-ball interaction zone" via a first loop to the β-ball (*black* in Fig. 1*B*) and via a second loop, which contains His-163, to the upper palm (*gray* in Fig. 1*B*). A second part of the finger is formed by a stretch of a loop between the palm and the β-ball that points toward the thumb region (the thumb is *green* in Fig. 1*A*) and corresponds to residues 229–244. Residues 223–229, which are at the interface between the upper palm and this loop of the finger, form the third loop in the finger-ball interaction zone (*brown* in Fig. 1*B*). Thus, three peptide chains contribute to the finger-ball interaction zone, which is shown in a close-up in Fig. 1*B*. His-163, which is part of the second chain, forms hydrogen bonds with both Asn-96 of the first and Gln-225 of the third peptide chains. Fig. 1*C* shows sequence alignments of these three segments, illustrating their

* This work was supported by Grant 31003A0-117717 from the Swiss National Science Foundation (to S. K.).

[S] The on-line version of this article (available at http://www.jbc.org) contains supplemental "Experimental Procedures," Figs. S1–S3, and additional references.

[1] To whom correspondence should be addressed: Dept. of Pharmacology and Toxicology, University of Lausanne, Rue du Bugnon 27, 1005 Lausanne, Switzerland. Tel.: 41-21-692-5422; Fax: 41-21-692-5355; E-mail: Stephan.Kellenberger@unil.ch.

[2] The abbreviations used are: ASIC, acid-sensing ion channel; hASIC1a, human ASIC1a; MTS, methanethiosulfonate; MTSET, 2-(trimethylammonium)-ethyl methanethiosulfonate; SSIN, steady-state inactivation; WT, wild type; MES, 4-morpholineethanesulfonic acid.

high degree of conservation. Because the finger domain contributes to pH-dependent gating (16–18), we hypothesized that the finger-ball interaction zone may be involved in ASIC gating. To understand the function of His-163 and its immediate surroundings, we introduced Cys residues by site-directed mutagenesis, probed them with Cd^{2+}, which can bind to Cys, and with methane thiosulfonate sulfhydryl reagents and analyzed the effects on channel expression and function. We show that His-163 and its immediate surrounding are critical for ASIC activity.

EXPERIMENTAL PROCEDURES

Site-directed Mutagenesis and Expression in Xenopus Oocytes—The original human ASIC1a cDNA construct was kindly provided by Dr. D. Corey. For oocyte expression, it had been subcloned into the pSDeasy vector. Point mutations were introduced using QuikChange (Stratagene, Amsterdam Zuidoost, Netherlands). Mutations were verified by sequencing (Synergene Biotech, Zurich, Switzerland). Expression in *Xenopus laevis* oocytes was carried out as described previously (18). Complementary RNAs were synthesized *in vitro* (mMESSAGE mMACHINE® SP6 kit, Ambion/Applied Biosystems, Rotkreuz, Switzerland). Oocytes were surgically removed from the ovarian tissue of female *X. laevis,* which had been anesthetized by immersion in MS-222 (2 g $liter^{-1}$; Sandoz, Basel, Switzerland). The oocytes were defolliculated, and healthy stage V and VI *Xenopus* oocytes were isolated and pressure-injected with 10 ng of cRNA or as indicated, and oocytes were kept in modified Barth solution during the expression phase. In a first series of experiments, several mutants had shown substantially lower acid-induced currents than ASIC wild type (WT). To allow a sufficiently high expression level of the mutants for functional analysis, we subcloned all mutant constructs in a vector for transcription that contained 5′- and 3′-untranslated regions of *Xenopus* β-globin, which is known to increase expression. As shown in supplemental Fig. S2, the use of the vector containing the 5′- and 3′-untranslated regions of *Xenopus* β-globin induced for both hASIC1a and a tested mutant (H163C) an increase in total and cell surface expression and increased the maximal current amplitude.

Cell Surface Protein Biotinylation and Western Blot Analysis—45 oocytes per condition were used, and the complete protocol was performed on ice. Oocytes were washed three times with modified Barth solution and then incubated in biotinylation buffer (10 mM triethanolamine, 150 mM NaCl, 2 mM $CaCl_2$, pH adjusted to 9.5) containing 1 μg/ml EZ-link sulfo-NHS-SS-Biotin (Pierce) for 15 min. The oocytes were then washed twice and incubated for 5 min in quench buffer (0.192 M glycine, 0.025 M Tris-HCl, pH 7.5, in modified Barth solution) to stop the biotinylation reaction. Oocytes were then lysed in 20 μl of lysis buffer per oocyte (1% Triton X-100, 500 mM NaCl, 5 mM EDTA, 50 mM Tris-HCl) and centrifuged at 12,000 rpm for 10 min at 4 °C. During the centrifugation step, 50 μl of ImmunoPure immobilized streptavidin beads (Pierce) per condition were washed with the lysis buffer, and the supernatant from centrifugation was added to the washed beads. The samples were incubated overnight at 4 °C. The samples were then centrifuged for 1 min at 14,000 rpm at 4 °C, and 40 μl of supernatant (corresponding to ~5% of the volume of the supernatant, representing the intracellular protein fraction) per condition were mixed with protein sample buffer, whereas the beads (containing biotinylated membrane protein fraction) were washed three times with the lysis buffer and then mixed with protein sample buffer. After boiling at 95 °C for 5 min, the samples were separated by 8% SDS-PAGE and transferred onto a nitrocellulose membrane (Schleicher & Schuell). The polypeptides were exposed to rabbit anti-ASIC1 primary antibody (MTY19, 1:1000) that recognizes a C-terminal epitope of hASIC1 (11) and goat anti-rabbit horseradish peroxidase (1:20,000, Amersham Biosciences) as secondary antibody and visualized using SuperSignal® West Dura Extended Duration Substrate (Pierce).

Electrophysiological Analysis—Electrophysiological measurements were performed 1–2 days after cRNA injection. Macroscopic currents were recorded using the two-electrode voltage clamp technique at a holding potential of −60 mV with a Dagan TEV-200 amplifier (Minneapolis, MN) equipped with two bath electrodes. Acidic (stimulation) solutions were applied once every minute for 5 s, and in-between the recording chamber was perfused with the conditioning solution. The standard bath solution contained in mM, 110 NaCl, 2.0 $CaCl_2$, 10 Hepes-NaOH (or MES-NaOH for pH < 6.8), and pH was adjusted with NaOH to the indicated values. Oocytes were placed in a recording chamber (300 μl) and perfused by gravity at 8 ml/min. The pipette solution contained 1 M KCl. Pipettes were pulled from borosilicate glass (Kimble Glass Inc., Germany). Kaleidagraph (Synergy software) was used to fit the pH activation curves to the Hill equation: $I = I_{max}/(1 + (10^{-pH\,50}/10^{-pH})^{nH})$, where I_{max} is the maximal current, pH 50 is the pH that induces half-maximal current, and n_H is the Hill coefficient. Steady-state inactivation curves were fitted by an analogous equation. The Cd^{2+} inhibition curves were fitted to the Hill equation: $I = I_0/(1 + ([Cd^{2+}]/IC_{50})^{nH})$, where I_0 is the current in the absence of Cd^{2+}, IC_{50} is the Cd^{2+} concentration that induces 50% inhibition, and n_H is the Hill coefficient.

The outside-out configuration of the patch clamp technique was used to obtain single-channel data. Before recording, the vitelline layer of the oocyte was removed. The extracellular solution for outside-out patches contained in mM, 110 NaCl, 0.5 $CaCl_2$, 0.5 $MgCl_2$, 10 Hepes-NaOH, and 10 MES-NaOH, with the pH adjusted to 7.4 or to the stimulating pH values. Changes of external solutions of outside-out patches were made using the Rapid Solution Changer RSC-200 (Biologic, Grenoble, France). The pipette solution contained in mM, 75 CsF, 17 *N*-methyl-D-glucamine, 10 EGTA, and 10 Hepes, pH 7.35. Pipettes for patch clamp experiments were pulled from borosilicate glass (World Precision Instruments, Stevenage, UK). In patch clamp experiments, currents were recorded with an EPC-9 patch clamp amplifier (HEKA Electronic, Lambrecht/Pfalz, Germany) and filtered at 100 Hz for analysis. Data are presented as mean ± S.E. Differences between WT and mutant forms of ASIC1a and between different treatments were analyzed by ANOVA followed by Dunnett post hoc test, using Kaleidagraph (Synergy software).

Reagents—Methanethiosulfonate reagents were obtained from Toronto Research Chemicals (North York, Canada), and other reagents were from Sigma, Fluka, or Applichem.

Homology Modeling—For the planning of the experiments and the interpretation of the data, a homology model of human ASIC1a was created based on the first chicken ASIC1 structure with Protein Data Bank code 2QTS (5) using the program Modeler 9 version 5 (19). Five models were generated and analyzed with Dope (20) and Anolea (21), and the model with the best overall score was selected. The homology model of human ASIC1a is very similar to the experimentally determined structure of chicken ASIC1a, due to very high sequence identity (90%). After superimposition on the Cα atoms, the root mean square deviation between the template crystal structure and the homology model was 0.5 Å. An analysis of the model by the program PROCHECK (22) showed that 92.4% of its residues are in the favorable regions, 7.5% in the generously and additionally allowed regions, and only 0.2% (2 residues) are in the disallowed regions of the Ramachandran plot. The modeling was performed within the Protein Modeling Facility of the University of Lausanne. Both published chicken ASIC1 structures share a high similarity in the region around His-163 (4, 5).

RESULTS

Protein and Current Expression of Finger-Ball Interaction Zone Mutants—His-163 and residues in its immediate environment in the finger-ball interaction zone were mutated to Cys. Among the mutated residues, we distinguished two categories based on their localization in the model of the ASIC structure (Fig. 1*B*; for model generation and testing see "Experimental Procedures"). Residues of category I are oriented toward the center of the finger-ball interaction zone (Asn-94, Asn-96, Gly-162, His-163, Gln-225, and Tyr-229) or form a contact between two of the strands (Ser-101 and Glu-228). These residues are shown as "*ball and stick*" in Fig. 1*B*. Except for Gly-162, they interact with other residues by H-bonds (*blue lines* in Fig. 1*B*). The other residues, constituting category II, are oriented toward the outside of this domain (Leu-95, Glu-97, Asp-164, Ile-224, and Gln-226; shown in "*stick*" representation in Fig. 1*B*).

WT or mutant ASIC1a was expressed in *X. laevis* oocytes. The expression of WT and mutant ASIC1a after injection of the same amount of cRNA was analyzed by Western blot. Before cell lysis, cell surface-expressed proteins were marked by biotinylation to allow their isolation. Fig. 2*A* shows Western blots of the intracellular pool and of the surface-expressed ASIC protein for ASIC1a WT and the different mutations. The ASIC1-specific antibody labeled a double band of an apparent molecular mass close to 70 kDa, corresponding to the single subunit. The existence of ASIC1a double bands has been reported previously and has been attributed to heterogeneous glycosylation (23). The intensity of the bands indicates that many mutants had expression levels that were comparable with that of WT except for the mutants N96C, S101C, and E228C, which showed strongly decreased protein expression. Fig. 2*B* shows the peak current amplitude induced by acidification to pH 4.5 as *black bars* for category I mutants and *gray bars* for category II mutants. The peak current amplitude of all mutant ASICs except for L95C and Q226C was decreased at least 3-fold with respect to WT (Fig. 2*B*), indicating that these mutations decreased channel expression or function. For most mutants, peak current amplitude correlated with the cell surface expression level (Fig. 2). Exceptions were H163C and Y229C, which had low current amplitudes despite a WT-comparable level of cell surface expression, indicating that these mutations reduced the current amplitude per channel number at the cell surface. Comparison of the unbound and the bound fractions demonstrated that mutants with low cell surface expression levels also had low intracellular expressions levels, indicating that the low cell surface expression was not due to an impaired insertion of the protein in the plasma membrane but rather due to an impaired protein synthesis or stability. This analysis shows that an intact finger-ball interaction zone is required for normal expression of the ASIC1a protein.

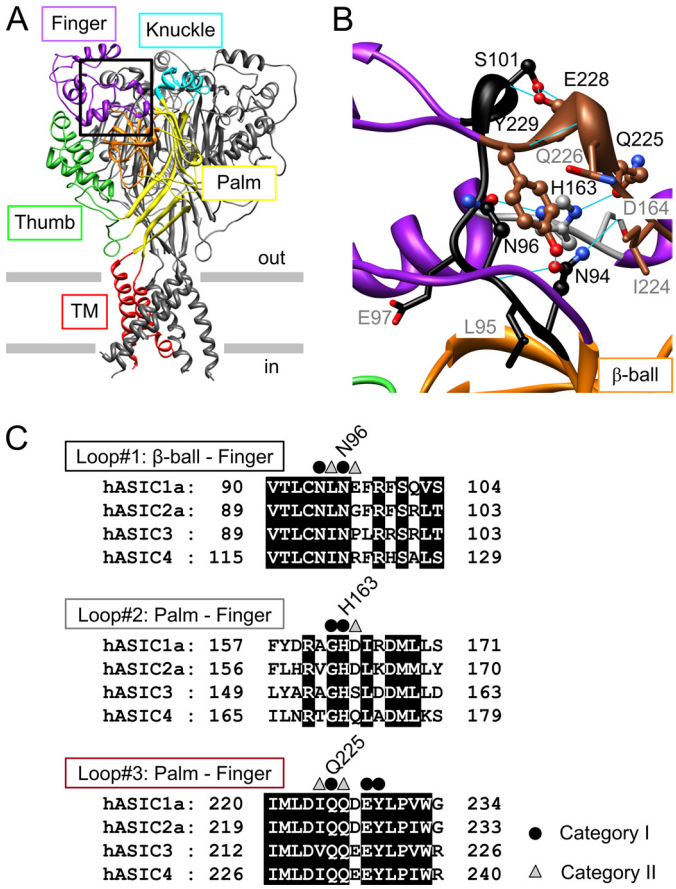

FIGURE 1. **Structure and conservation of the finger-ball interaction zone in ASIC1a.** *A*, structure of hASIC1a established by homology modeling based on chicken ASIC1 (Protein Data Bank code 2QTS). One of the three ASIC subunits is shown in color, identifying different parts of ASIC subunits (*red*, transmembrane segments; *yellow*, palm; *orange*, β-ball; *green*, thumb; *purple*, finger; *turquoise*, knuckle). *B*, view of the finger-ball interaction zone with loop 1 in *black*, loop 2 in *gray*, and loop 3 in *brown*. The side chains of the residues mutated in this study are represented as "*ball-and-stick*" (category I residues, see text) and as "*stick*" (category II residues). Hydrogen bonds predicted in Chimera (33) are indicated as *blue solid lines*. *A* and *B* are presented in stereo view in supplemental Fig. S1. *C*, sequence alignment of the three loops forming the finger-ball interaction zone, highlighting the amino acids substituted in this study. The amino acid sequences of the extracellular regions of human ASIC1a, -2a, -3, and -4 are aligned (GenBank™ accession numbers are as follows: hASIC1a, 21536349; hASIC2a, 1280439; hASIC3, 3747101; and hASIC4, 8346834). Category I residues are marked by ● and category II residues by △.

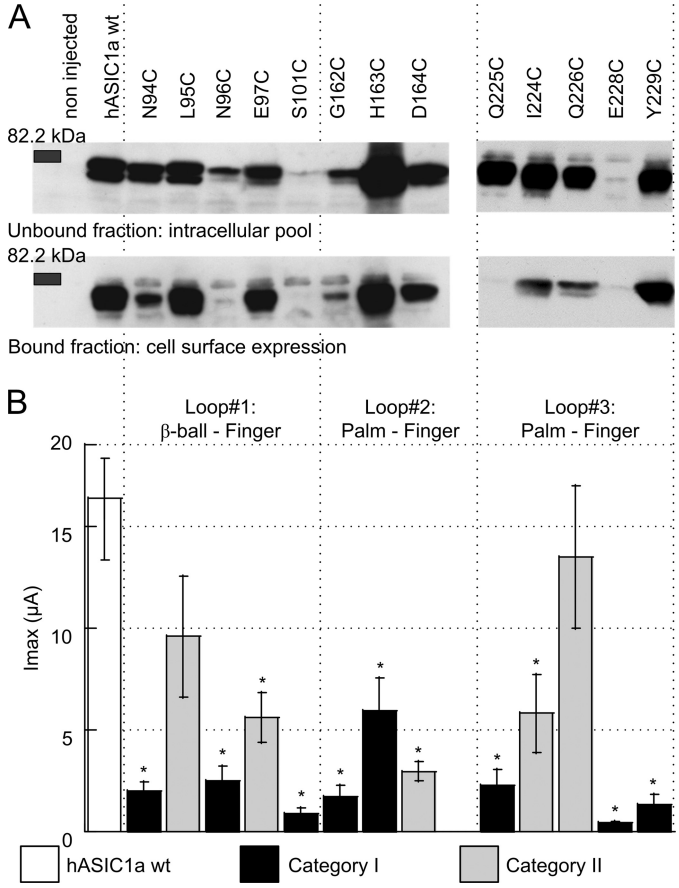

FIGURE 2. **ASIC protein and current expression.** *A,* representative Western blots of the cell surface expression of WT and mutant ASIC1a. Cell surface proteins were isolated by biotinylation, as described under "Experimental Procedures," from 45 ASIC1a-expressing oocytes 1 day after injection of 10 ng of cRNA. ASIC1a (~70 kDa) was visualized by a specific antibody (MTY19) that recognizes a C-terminal epitope of hASIC1 (11). Representative blots of the unbound and the bound fraction from 1 of ≥3 similar experiments per channel type are shown. *B,* peak current amplitude of ASIC1a WT and mutants (as indicated at the *top* of the figure) induced by acidification to pH 4.5 at a holding potential of −60 mV, 1–2 days after injection of 10 ng (WT) or 10–50 ng of cRNA per oocyte (mutants; $n = 6–28$, shown as mean ± S.E.). *, different from ASIC WT, $p < 0.05$ (ANOVA and Dunnett post hoc test).

Cadmium Interacts with Engineered Cys Residues in the Finger-Ball Interaction Zone and Decreases ASIC Current—We exposed ASIC1a WT and Cys mutant-expressing oocytes to Cd^{2+} or to the sulfhydryl reagent [2-(trimethylammonium)ethyl]methanethiosulfonate (MTSET) to test whether these residues were accessible and whether the binding of Cd^{2+} or the chemical modification affected channel function. Cadmium inhibited at micromolar concentrations some of the mutants completely, although at 10 mM it inhibited only ~30% of the ASIC1a WT current, as illustrated by the inhibition curves in Fig. 3*A*. The inhibition by Cd^{2+} was rapidly reversible upon washout of Cd^{2+} (data not shown). Because Cd^{2+} shifted the pH dependence of activation of some mutants (see below, Fig. 6*B*), we measured Cd^{2+} inhibition as the inhibition of the pH 4.5-induced peak current amplitude. Acidification to pH 4.5 induced maximal current responses in all mutants. The observed current inhibition by Cd^{2+} (Fig. 3, *A* and *B*) therefore represents the inhibition of the maximal peak current amplitude and is not due to possible shifts in the pH dependence of activation induced by Cd^{2+}. Concentrations of half-maximal inhibition (IC_{50}) obtained from this analysis are shown in Fig. 3*B*. In Fig. 3*B*, mutations of category I and II residues are shown as *black* and *gray symbols*, respectively. The IC_{50} values were lower as compared with WT for all mutants except for L95C, E97C, D164C, and I224C, indicating that except for these four residues the engineered Cys residues interacted with Cd^{2+}. Category I mutants generally had a higher apparent affinity for Cd^{2+} than category II mutants. Most of the category I residues point toward His-163 and may, when mutated to Cys, form a Cd^{2+}-binding site together with His-163. We hypothesized that for this reason several category I residue mutations had a higher apparent Cd^{2+} affinity than H163C. We tested this hypothesis for two residues, Asn-96 and Gln-225 by mutating His-163 to Asn and combining this mutation with the mutation N96C or Q225C. We had chosen the conservative mutation H163N because this mutant was reported as expressing WT-comparable currents and pH dependence (16) and therefore should allow the construction of functional double mutants. The H163N mutation reduced the Cd^{2+} affinity by ~5-fold as compared with the H163C mutant, but it still showed 10-fold higher Cd^{2+} affinity than the WT (*filled squares* in Fig. 3*B*). The IC_{50} of Cd^{2+} inhibition of the double mutant H163N/N96C was not different from the single N96C mutant (Fig. 3*B*); however, the combination of the Q225C mutation with the H163N mutation increased the IC_{50} by ~30-fold. This indicates that the high apparent affinity for Cd^{2+} inhibition of Q225C depends on the presence of His-163. These two control experiments show that at least for some, but clearly not all category I residues, the high apparent Cd^{2+} affinity was due to a chelation of Cd^{2+} between the engineered Cys and His-163. S101C and E228C displayed the lowest apparent Cd^{2+} affinity of category I mutants. They form an H-bond connecting loop 1 and 3 and are too far from His-163 to chelate Cd^{2+} together with His-163. Gln-226 points away from this domain and interacts with the knuckle domain of the adjacent subunit. It may form a Cd^{2+}-chelating site together with residues from the neighboring knuckle, which might be the cause of its relatively high apparent affinity for Cd^{2+}.

Sulfhydryl Reagent MTSET Modifies Selected Engineered Cys Residues of the Finger-Ball Interaction Zone in a State-dependent Manner—To measure a more direct effect of sulfhydryl modification, independent of chelation between more than one residue, we exposed oocytes expressing the WT or mutant ASIC1a to the positively charged sulfhydryl reagent MTSET. MTSET fits into a cylinder with a radius of 3 Å and a height of 10 Å and is much larger than Cd^{2+}, whose Pauling radius is 0.65 Å. MTSET forms a disulfide bond with Cys residues, thereby adding the trimethylammonium-ethyl group. Fig. 3*C* shows current traces of responses to acidic stimulation of different pH values of an oocyte expressing ASIC1a H163C, before and after a 5-min exposure to 1 mM MTSET. In the H163C mutant, MTSET modification strongly inhibited the peak current amplitudes (note the difference in scale of the traces in Fig. 3*C*), demonstrating that the residue is accessible and that its modification impaired channel function. Fig. 3*D* summarizes the effects of MTSET on the maximal peak current amplitude of different mutants. Category II mutants showed less than 30%

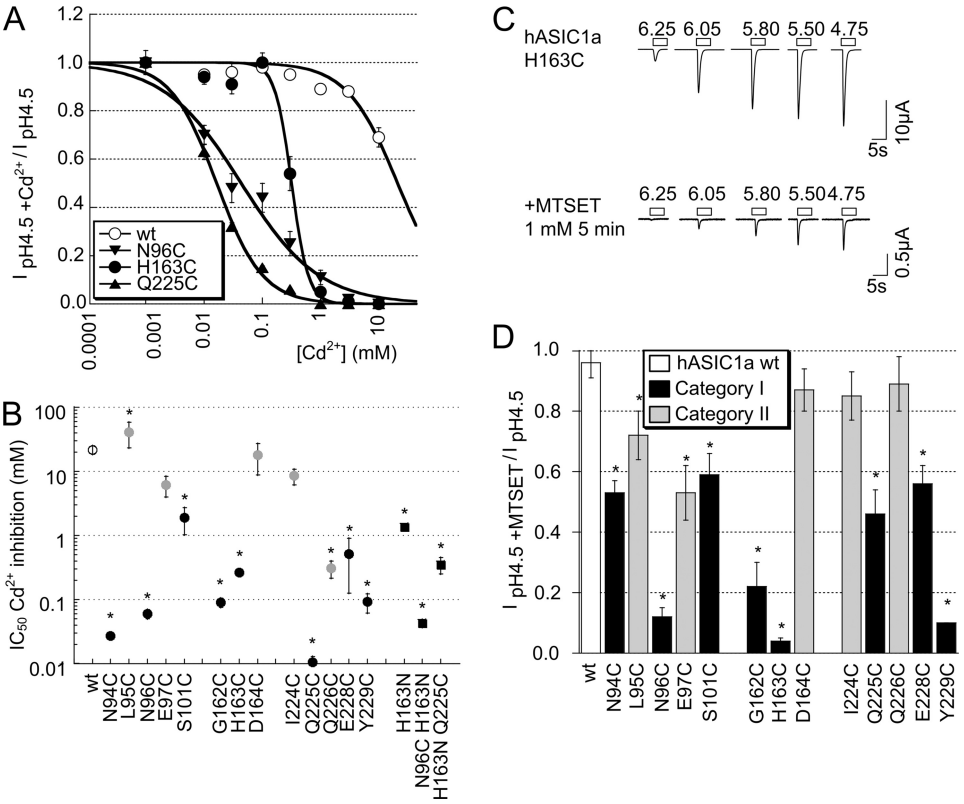

FIGURE 3. **Inhibition of ASIC1a WT and mutants by external Cd^{2+} and MTS reagents.** *A*, Cd^{2+} inhibition curves of pH 4.5-induced current in oocytes expressing ASIC1a WT (○, $n = 10$), N96C (▼, $n = 9$), H163C (●, $n = 4$), and Q225C (▲, $n = 3$). The *lines* represent fits to the Hill equation (see "Experimental Procedures"). *B*, IC_{50} values of Cd^{2+} inhibition of WT and mutant ASIC1a ($n = 3$–10, mean ± S.E.). For several points, the error was smaller than the symbol. *, IC_{50} values are different from WT, $p < 0.05$ (ANOVA and Dunnett post hoc test). *C*, representative current traces of oocytes expressing ASIC1a H163C obtained by a 5-s acidification to the indicated pH values at a holding potential of −60 mV before and after a 5-min incubation with 1 mM MTSET. *D*, normalized pH 4.5-induced ASIC1a peak current amplitudes (mean ± S.E., normalized to current amplitude before exposure), after a 5-min exposure to 1 mM MTSET ($n = 3$–7). *, inhibition by MTSET different from WT, $p < 0.05$ (ANOVA and Dunnett post hoc test).

inhibition except for E97C, which was inhibited by ~50%. In contrast, all category I residue mutants were inhibited by more than 40%. We determined the kinetics of the decrease of the pH 5.5-induced current amplitude for most category I mutants. For this, we induced channel activation every 60 s by a 5-s acidification to pH 5.5, and we added MTSET between these acidification steps at a concentration <1 mM (*e.g.* 0.15 mM for Q225C) that allowed resolution of the kinetics of the MTSET-induced current decrease. Typical current traces of such an experiment are shown in supplemental Fig. S3*A*, and the kinetics of the pH 5.5-induced current decrease of three mutants are shown in supplemental Fig. S3*B*. From the fit to the kinetics, we calculated the rate of MTSET-induced current decrease in units of $min^{-1}\ M^{-1}$ to allow quantitative comparison of the kinetics measured at different MTSET concentrations. This analysis yielded reaction rates of ~1500–3000 $min^{-1}\ M^{-1}$ for most mutants, a slightly higher rate for E228C, and an ~10-fold higher rate for N96C (supplemental Fig. S3*C*). For the mutant with the lowest observed rate, H163C, 1540 ± 154 $min^{-1}\ M^{-1}$, exposure to 1 mM MTSET results in 95% of maximal modification after 2 min and 100% after 5 min, as calculated based on a mono-exponential time course. This indicates that for these mutants modification was complete after 5 min of exposure to 1 mM MTSET. The 10-fold higher rate of current decrease in N96C is either due to better accessibility or to higher reactivity of the Cys at position 96.

To test whether His-163 and close residues were also accessible to reagents larger than MTSET, we exposed the His-163 and Gln-225 mutants to 2-(triethylammonium)-ethyl methanethiosulfonate and 2-(tributylammonium)-ethyl methanethiosulfonate, which contain a triethylammonium and tributylammonium group, respectively, as illustrated in Fig. 4*A*. These reagents decreased the maximal peak current amplitude to a similar degree as did MTSET (Fig. 4*B*), indicating that these reagents can equally well reach H163C and Q225C as does MTSET.

The rate of current decrease due to MTSET exposure depends on the accessibility of the engineered Cys residue and may differ at different functional states of the channels, if conformational changes occur in the environment of the residue that reacts with MTSET. The crystal structure on which the homology model of the hASIC1a structure is based was obtained at acidic pH and therefore represents most likely the inactivated conformation of the channel (5). In the experiments described in Figs. 3 and 4*B*, the reagent was added to the closed channels (at pH 7.4). To test whether the accessibility of these engineered residues is different between the closed and the inactivated state, we exposed oocytes expressing selected mutants to 1 mM MTSET during 2 min at either pH 7.4, 7.2, 7.0, or 6.8. The relatively short exposure time was chosen because a longer exposure duration (and therefore highly saturating conditions) might allow for compensation of differences and would therefore reduce the discriminative power. The incubation pH did not affect the current decrease due to MTSET exposure in the mutants N94C, S101C, Q225C, and E228C (Fig. 4*C*). There was a small current decrease in the ASIC1a WT at pH 7.0. The fact that the MTSET-induced current decrease did not depend on the MTSET incubation pH for these mutants and that there was only a small effect of pH on the WT current decrease indicates that in the pH range studied there is at most a very small intrinsic pH dependence of the sulfhydryl reaction. Interestingly, the MTSET effect was strongly reduced at lower incubation pH in three mutants, N96C, G162C, and H163C (Fig. 4*C*). The hASIC1a WT undergoes inactivation if exposed to pH < 7.3, with a pH of half-maximal inactivation (pHIn50) around 7.1, and for the mutants studied the pHIn50 was in the range of 7.0–7.2 (Fig. 5, *C* and *D*). Therefore, the observed reduction in the effect of MTSET at pH <7.2 in the case of G162C and

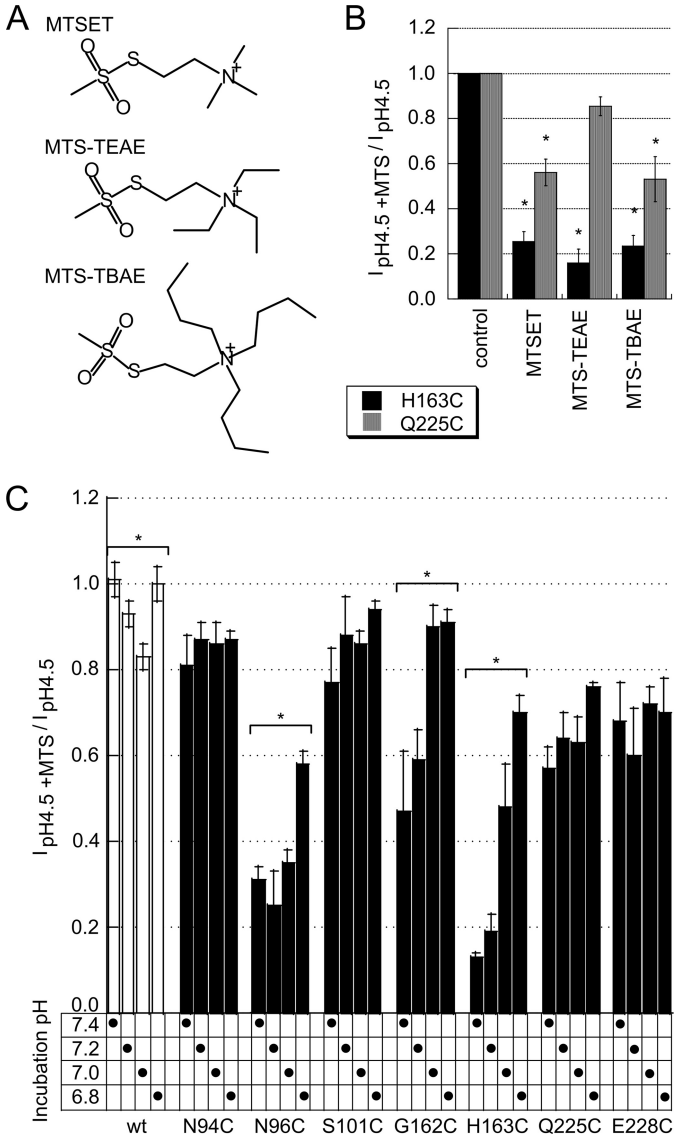

FIGURE 4. **Inhibition by large MTS reagents and state-dependent accessibility of MTSET.** *A,* structures of the MTS reagents used in experiments described in *B*. *B,* normalized pH 4.5-induced ASIC1a peak current amplitudes (mean ± S.E., normalized to current amplitude before exposure) after a 2-min exposure to different MTSET reagents at 1 mM (n = 3–4, mean ± S.E.). *, inhibition by MTS reagent different from control (no reagent), $p < 0.05$ (ANOVA and Dunnett post hoc test). *C,* normalized pH 4.5-induced ASIC1a peak current amplitudes (mean ± S.E., normalized to current amplitude before exposure) after a 2-min exposure to 1 mM MTSET at the pH of MTSET exposure indicated (n = 3–4, mean ± S.E.). *, inhibition by MTSET depends on incubation pH, $p < 0.05$ (ANOVA).

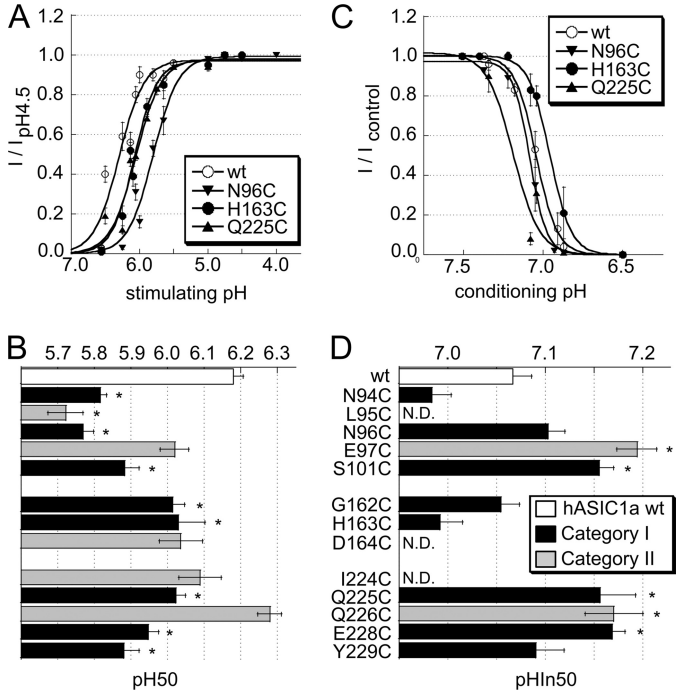

FIGURE 5. **pH dependence of ASIC1a activation and SSIN.** *A,* pH dependence of activation of ASIC1a WT (○) and the mutants N96C (▼), H163C (●), and Q225C (▲) (n = 7–14). Currents were normalized to the peak current measured at pH 4.5. The *lines* represent fits to the Hill equation (see "Experimental Procedures"). *B,* pH of half-maximal activation pH 50 of ASIC1a WT and mutants, n = 3–14. *, pH 50 different from WT pH 50, $p < 0.05$ (ANOVA and Dunnett post hoc test). The *y* axis labeling on *B* is identical to that of *D*. *C,* pH dependence of SSIN of ASIC1a WT (○) and the mutants N96C (▼), H163C (●), and Q225C (▲) (n = 6–12). Currents were induced by a 5-s acidification to pH 4.5 after exposure for 55 s to the conditioning pH. The current normalized to the condition with the most alkaline conditioning pH is plotted as a function of the conditioning pH. *D,* pH for half-maximal inactivation (pHIn50) of ASIC1a WT and mutants, n = 4–16. *, pHIn50 different from that of WT, $p < 0.05$ (ANOVA and Dunnett post hoc test), *N.D.*, not determined. Data are presented as mean ± S.E.

H163C and at pH < 7.0 in N96C strongly suggests that the accessibility or the reactivity of these residues is reduced upon inactivation, most likely due to conformational changes in the finger-ball interaction zone.

Effects of Mutations on ASIC pH Dependence—The observed inhibition of ASIC currents by Cd^{2+} and MTS reagents could be due to the following: 1) a change in the pH dependence of the channel; 2) a reduced probability of opening upon acidification, thus an effect on gating; or 3) a decrease in unitary channel conductance. To test whether the mutation and subsequent exposure to Cd^{2+} or MTSET affect pH dependence, we determined first the pH dependence of ASIC1a WT and mutants. The pH dependence of activation was measured by exposing WT and mutant ASICs to solutions of different pH values from a conditioning solution (*i.e.* the solution between the short acidic stimulations) of pH 7.4. For ASIC1a WT and selected mutants, the normalized current in control conditions is plotted as a function of the stimulation pH in Fig. 5*A*. The pH-current relationship is characterized by the pH that induces 50% of the maximal peak current amplitude, pH 50, and the Hill coefficient n_H, which is determined by the steepness of the curve. The values of these parameters were obtained from fits of the experimental data to the Hill equation (see "Experimental Procedures"). The pH 50 values are plotted for WT and the different mutants in Fig. 5*B* (*black*, category I; *gray*, category II mutants). Many mutations shifted the pH 50 to more acidic values as compared with WT, indicating that these mutant channels were already without sulfhydryl modification less H^+-sensitive than ASIC WT. These shifts were of ~0.1–0.4 pH units, corresponding to a 1.25–2.5-fold decrease in apparent H^+ affinity, and they were most pronounced in mutations of the first loop.

The steady-state inactivation (SSIN) represents the direct transition from the closed to the inactivated state during prolonged exposure to moderately acidic pH. For ASIC1a, the pH

of half-maximal inactivation (pHIn50) is ~7.1. Therefore, at pH values more acidic than 7.4, an increasing fraction of ASIC1a channels is in the inactivated conformation from which they cannot be opened by acidification. SSIN determines the fraction of channels that are available for opening and is therefore of physiological importance. An alkaline shift of the pH dependence of SSIN due to a mutation or the sulfhydryl modification may cause a decrease in peak current amplitude. To measure the pH dependence of SSIN, we exposed ASIC1a-expressing oocytes during 55 s to the conditioning pH in the range of 8.0 to 6.6, before switching to pH 4.5 for ASIC activation. In Fig. 5*C*, the normalized current is plotted as a function of the conditioning pH for ASIC1a WT and three mutants. The pH-inducing half-maximal inactivation (pHIn50) values were determined from the current-pH relationship by fitting the data to a modified Hill equation (see "Experimental Procedures"). We measured the pHIn50 values of all mutants whose maximal peak current amplitude had been shown to be decreased by exposure to MTSET (Fig. 3*D*) or whose IC_{50} value of Cd^{2+} inhibition was ≤2 mM (Fig. 3*B*). Several mutations in loop 1 and 3 induced alkaline shifts, which were of the order of 0.1 pH units (Fig. 5*D*).

Effects of MTSET and Cd^{2+} on pH Dependence—The effect of MTSET modification on the pH dependence of activation was determined for each mutant in a direct comparison to the control condition. The shift in pH 50, ΔpH 50, was calculated as the difference of pH 50 after MTSET-pH 50 before MTSET and is plotted in Fig. 6*A*. The shift in pH 50 by Cd^{2+}, determined in an analogous way, is plotted in Fig. 6*B*. These experiments were done at Cd^{2+} concentrations close to the Cd^{2+} IC_{50}, thus 50 μM for N94C, N96C, Q225C, and Y229C and 500 μM for S101C, G162C, H163C, Q226C, and E228C. Exposure to MTSET induced an acidic shift of ~0.2–0.3 pH units in N96C and E97C. Acidic shifts of pH 50 values in the presence of Cd^{2+} that were significantly different from that of WT ASIC1a were found in the mutant N96C and G162C (Fig. 6*B*). pH 50 shifts were found in both category I and II mutants, suggesting that the effect on the pH 50 does not correlate with the proximity or the orientation relative to His-163.

The shifts in the pH dependence of SSIN were determined by direct comparison between the control condition and exposure to Cd^{2+} or MTSET and are shown in Fig. 6, *C* and *D*, for MTSET and Cd^{2+}, respectively. MTSET induced an acidic pHIn50 shift of ~0.15 pH units in E97C and Q225C. Cadmium at 50 μM induced an alkaline shift of pHIn50 in Q225C. At 500 μM, Cd^{2+} induced a small acidic shift in WT pHIn50. Such an influence of divalent cations on ASIC1a pH dependence has been described previously (24). At 500 μM, Cd^{2+} induced an acidic shift that was significantly larger than the one observed in WT in G162C, Q226C, and E228C. The effect of Cd^{2+} on E97C pH dependence was not determined, because E97C has a very low apparent affinity for Cd^{2+} (Fig. 3*B*).

In summary, Cd^{2+} and MTSET induced shifts in the pH dependence of several of the mutants tested. Are these shifts the cause of the observed current decrease after exposure to Cd^{2+} or MTSET? Regarding ASIC activation, three mutants on the first loop, L95C, N96C, and E97C, showed the lowest pH 50 value after MTSET or Cd^{2+} exposure. Their pH 50 after modification was around 5.7, as can be calculated by adding the observed shift (Fig. 6, *A* and *B*) to the pH 50 of the mutant (Fig. 5*B*). The activation curves of these and the other mutants saturated at pH values more alkaline than 4.5 (data not shown); thus pH 4.5 still induced a maximal peak current amplitude, indicating that the observed decrease in pH 4.5-induced current (Fig. 3, *B* and *D*) is not due to a shift in the pH dependence of activation. An alkaline shift of the pH dependence of SSIN might decrease the ASIC current amplitude, if the modified channel is already partially inactivated at the conditioning pH used in the experiments, which was 7.4. Except for Q225C, exposure to Cd^{2+} or MTSET induced an acidic shift or had no effect on pHIn50 in all mutants tested. Steady-state inactivation developed at pH values <7.4, and a shift in pHIn50 is therefore not the cause of the observed current decrease.

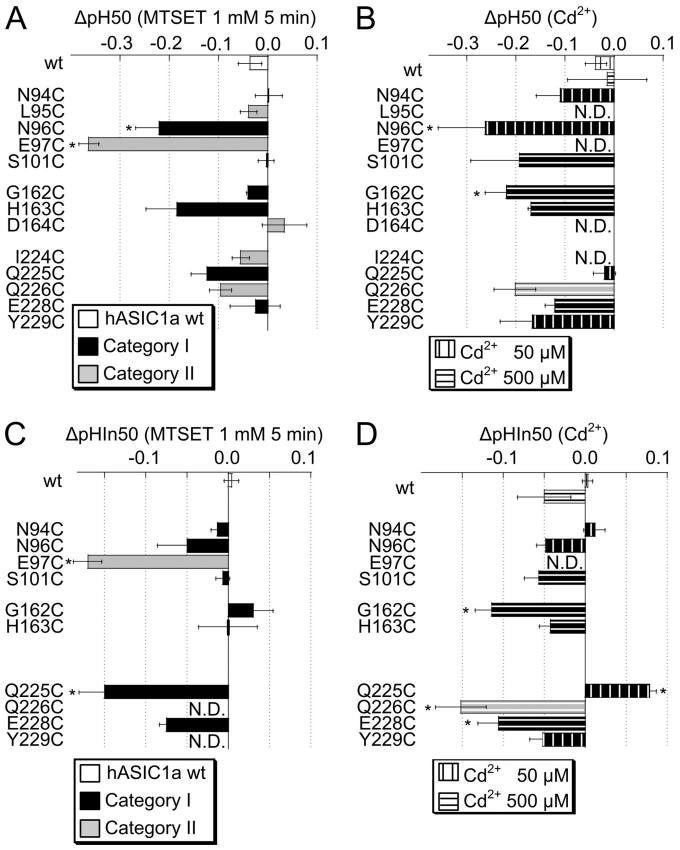

FIGURE 6. **Effects of Cd^{2+} and MTSET on ASIC pH dependence.** *A*, shift in pH of half-maximal activation, ΔpH 50 by 5-min exposure to 1 mM MTSET, calculated as the pH 50 after exposure to MTSET −pH 50 before exposure to MTSET, $n = 3–6$. *B*, shift in pH of half-maximal activation, ΔpH 50 in the presence of 50 μM (*vertically hatched bars*) or 500 μM Cd^{2+} (*horizontally hatched bars*) compared with situation without Cd^{2+}, calculated as in *A*. $n = 3–4$. * in *A* and *B*, ΔpH 50 different from WT ΔpH 50, $p < 0.05$ (ANOVA and Dunnett post hoc test). *C*, shift in pH of half-maximal inactivation, ΔpHIn50 by 5-min exposure to 1 mM MTSET, calculated as the pHIn50 after exposure to MTSET −pHIn50 before exposure to MTSET, $n = 3–8$. *D*, shift in pH of half-maximal inactivation, ΔpHIn50 in presence of 50 μM (*vertically hatched bars*) or 500 μM Cd^{2+} (*horizontally hatched bars*) compared with situation without Cd^{2+}, calculated as in C. $n = 3–4$. * in *C* and *D*, ΔpHIn50 different from WT ΔpHIn50, $p < 0.05$ (ANOVA and Dunnett post hoc test). *N.D.*, not determined.

Unitary Current Amplitude Is Similar in WT and Mutants—As discussed above, changes in channel gating or conductance may be a possible cause for the observed decrease in peak cur-

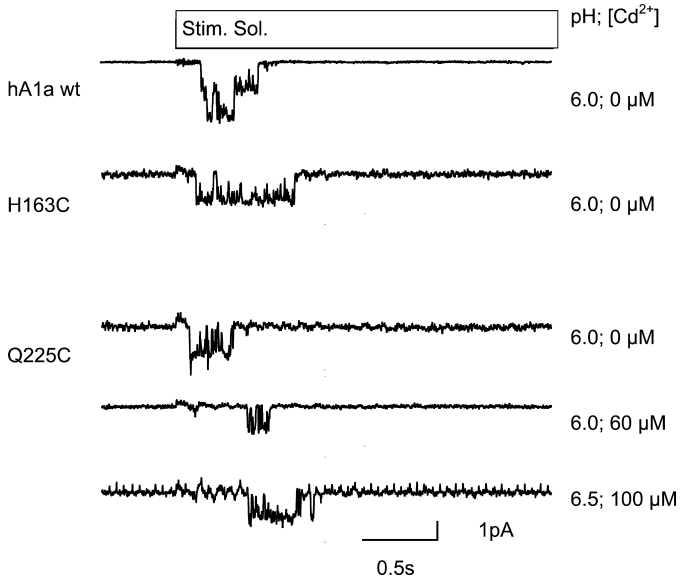

FIGURE 7. **Single-channel currents in WT and mutant ASIC1a.** Representative acid-evoked single channel traces recorded from excised outside-out patches of ASIC1a-expressing oocytes as described under "Experimental Procedures." *Stim Sol*, stimulation solution.

rent amplitudes after mutation or modification of residues in the finger-ball interaction zone. Although we have not carried out a single-channel analysis of the gating of WT and mutant ASIC, some information can be obtained from the analysis of the macroscopic current. Acceleration of the inactivation rate may decrease the peak current amplitude. We have measured the time course of open-channel inactivation, which depends on the inactivation rate, from current traces at stimulation pH of 6.0 and 4.5. Although we observed tendencies to an acceleration of open-channel inactivation in N96C, S101C, G162C, and H163C compared with WT, and tendencies to a slowing in L95C, D164C, I224C, and E228C, these changes were not significant (supplemental Fig. S4). Exposure to MTSET did not further change significantly the open-channel inactivation time course in any of the mutants. Therefore, this analysis does not provide evidence for a role of changed channel kinetics in the observed current reduction due to the mutations or the exposure to Cd^{2+} or MTSET.

To test whether a change in unitary channel conductance could be at the origin of the decreased current amplitude induced by the mutation and/or the subsequent modification, we measured unitary currents from excised outside-out patches from oocytes expressing ASIC1a WT or the H163C or Q225C mutant. As illustrated by representative current traces in Fig. 7, the mutations tested did not decrease the unitary current amplitude measured at −60 mV, which was in the absence of reagents −1.78 ± 0.39 pA for ASIC1a WT, −1.76 ± 0.36 pA for Q225C, and −1.66 ± 0.38 pA for H163C. We have measured Q225C channel currents in the presence of 60 or 100 μM Cd^{2+}, which inhibited the pH 4.5-induced macroscopic current by ~70–85% (Fig. 3*A*). At these concentrations, the unitary current was not significantly inhibited (Fig. 7). The unitary current amplitude in the presence of 60 μM Cd^{2+} was −1.85 ± 0.25 pA (n = 48–392).

DISCUSSION

The residue His-163 is located at the interface between three structural domains of the ASIC extracellular loop in a region that is highly conserved in ASICs. We have analyzed the role of this finger-ball interaction zone in ASIC function. Mutation and/or site-specific chemical modification of His-163 and many of the residues oriented toward the center of the finger-ball interaction zone (category I residues) led to a decrease in ASIC expression and maximal current amplitude and also changed the pH dependence of the channels. The decrease in ASIC maximal peak current amplitude after exposure to Cd^{2+} or to MTS reagents was, however, not due to shifts in ASIC pH dependence or a decrease in unitary channel conductance nor was it due to a change in the number of channels at the cell surface. This suggests that Cd^{2+} binding to or MTSET reaction with engineered Cys residues in the finger-ball interaction zone reduces the channel open probability. For three mutants, the effect of MTSET was smaller when the reagent was applied in pH conditions at which ASICs are inactivated, suggesting that inactivation induces conformational changes in the finger-ball interaction zone.

Expression of Mutant Channels—Many of the residues in the finger-ball interaction zone are rather hydrophilic. Mutation to the small, hydrophobic Cys is therefore expected to disrupt some interactions, as *e.g.* the H-bonds, because the mutation to Cys removed in most cases the atoms involved in H-bonds. The loss of H-bonds may be the cause of the observed reduction in ASIC currents. Indeed, when some of the residues that have been mutated in our study were mutated to other hydrophilic residues, thereby most likely preserving the H-bonds, neither the expression nor the function was changed. Examples are the H163N and E228Q mutations in rat ASIC1a (16). However, it cannot be completely excluded that some of these mutations might destabilize the protein structure in a nonspecific way.

Mechanisms by Which Cd^{2+} and MTS Reagents Decrease ASIC Currents in the Mutants—The changes in channel function observed after MTSET reaction or in the presence of Cd^{2+} developed rapidly (order of minutes for MTSET and of seconds for Cd^{2+}). In the case of Cd^{2+}, they were also completely and rapidly reversible. Therefore, an effect on the ASIC cell surface expression can be excluded. The maximal current amplitude might be decreased by a shift in pH dependence, but only if the shift of the activation is so large that at the stimulating pH measured (pH 4.5) the maximal current amplitude is not attained. Alternatively, the maximal current amplitude could be decreased by an alkaline shift of the pH dependence of SSIN, if the induced shift leads to inactivation of a fraction of the channels at the conditioning pH of the measurement, thus at pH 7.4. Although shifts in the pH dependence were observed due to sulfhydryl reaction in some mutants, they were too small or of the wrong sign (*i.e.* acidic shift of pHIn50) to be the cause of the observed decrease in current. Although the finger-ball interaction zone is far from the transmembrane and intracellular domains that have been shown to contribute to pore functions in epithelial Na^+ channel/degenerin channels (25, 26),

we tested whether mutation or modification changed the unitary current amplitude. The single-channel measurements, carried out with selected mutants, have shown that the unitary current amplitude was not decreased in mutants as compared with WT and was not decreased in the presence of Cd^{2+} concentrations that strongly inhibit the macroscopic current.

Therefore, we conclude by exclusion of other possibilities that binding of Cd^{2+} and sulfhydryl modification by MTS reagents interferes with the gating mechanisms. The single-channel measurements carried out with the aim of determining the unitary conductance do not allow a quantitative analysis of channel gating. ASICs have been proposed to function in different gating modes with different open probabilities (27). It is possible that Cd^{2+} binding to or modification by MTSET of engineered Cys residues in the finger-ball interaction zone may put ASICs preferentially in a low open probability gating mode. Alternatively, it might reduce the probability of channel opening upon acidification, thus by acting on a ligand-independent transition that follows ligand binding. Our data do not allow us to distinguish between these two possibilities.

The remaining current after exposure to MTSET or in the presence of Cd^{2+} had a modified pH dependence in some mutants, indicating that although these channels had been modified by MTSET or complexed by Cd^{2+}, they were not completely inhibited. Because there are three finger-ball interaction zones per channel, it is possible that the channels with changed properties have been incompletely modified or bind Cd^{2+} only in one or two subunits.

Interface between Finger, β-Ball, and Upper Palm—The importance of the finger domain for the ASIC pH dependence has previously been shown. Three residues in the lowest α-helix of the finger, Lys-105, Asn-106, and Asp-107, profoundly affect the pH dependence of ASIC activation and SSIN when mutated (16, 17), and cleavage by trypsin at Arg-145 on the uppermost α-helix of the finger shifts the pH dependence of both activation and inactivation (18). Three of the four ends of the two peptide chains that form the finger pass through the finger-ball interaction zone, of which His-163 is the central residue. His-163 forms hydrogen bonds to residues on the two other loops connecting to the finger, Asn-96 on the first, and Gln-225 on the third loop. The finger is thus connected to the rest of the protein via the three strands passing through the finger-ball interaction zone and, in addition, through the continuation of the third of these strands that loops to the thumb region where it likely contributes to pH sensing (5, 14) and connects back to the β-ball.

Alternatively, the finger-ball interaction zone might not only link different domains but might itself contribute to ASIC pH sensing. The finger-ball interaction zone contains the potential pH-sensing residues His-163, Glu-228, Glu-97, and Asp-164. Glu-97 takes a special place among these residues, as it points away from the finger-ball interaction zone toward the thumb domain, where it may contribute to a network of protonable residues (5). In addition, it had previously been shown to contribute to Psalmotoxin binding (28). Mutation of His-163 to Cys induced significant changes in ASIC pH dependence and might therefore be a pH sensor. However, a more conservative mutation of this residue to Asn, which also should disrupt its role as pH sensor, did not affect ASIC1a pH dependence in a recent study (16), arguing against such a role of His-163. We have analyzed the pH dependence of the conservative mutants E228Q and D164N and found no change in activation or SSIN pH dependence relative to WT (34). Therefore, we conclude that the finger-ball interaction zone does not sense the pH by itself, except for a contribution of Glu-97. Rather, it acts as a linker that connects different domains involved in sensing and the parts of the protein that contain the channel gate. It is conceivable that if this linker is more resistant or less well adapted for transmitting the conformational changes induced by proton binding further toward the gate, due to mutation or modification, higher ligand concentrations are needed to "force" the channel opening, which would explain the shifts in pH dependence. An illustration of such a mechanism has been provided by a study of the link between the extracellular loop and the first transmembrane segment in rat ASIC1a (29). The residue Trp-288 (Trp-287 in hASIC1a) is located at the lowest position of a loop connecting the thumb with the palm. Trp-288 points down on Tyr-72 (Tyr-71 in hASIC1a) at the extracellular end of the first transmembrane segment. Li *et al.* (29) showed that these two residues are critical for ASIC function and that their mutation induced strong shifts in ASIC pH dependence, although these two residues can clearly not be pH sensors.

Conformation of the Finger-Ball Interaction Zone—Cadmium showed a higher apparent affinity for category I than the category II mutants. Cadmium can be complexed by Cys and His residues similarly to Zn^{2+}, which is in the same column of the periodic table. It is likely that in some of these mutants the Cd^{2+} ion was complexed by the introduced Cys and by His-163. Our experiments with selected mutants showed that this is the case for Q225C but not for N96C. In Cd^{2+}-chelating peptides, the distance between Cd^{2+} and the chelating sulfur atom of the Cys is ~2.5 Å, and the distance to the nitrogen atom of the His residue is ~2.3 Å (30). For comparison, hydrogen bonds have center-to-center distances of the involved nitrogen and oxygen atoms of ~3 Å. It is likely that the Cd^{2+} binding enforced the interaction between two chains of the finger-ball contact zone, *e.g.* between H163C of loop 2 and Q225C of loop 3, but did this in a conformation that was different from the normal (WT) conformation of this region. According to the structure, besides the Asn-96–His-163–Gln-225 axis, there are in the finger-ball interaction zone two pairs of residues whose side chains point toward each other, Ser-101 to Glu-228 and Asn-94 to Tyr-229. Interestingly and consistent with this relative orientation, the Cd^{2+} IC_{50} values were similar between the residues engaged in a pair when either one or the other residue was mutated.

Reaction with MTSET induced a stronger inhibition of category I than of category II mutants, confirming that the side chains oriented toward the center of the finger-ball interaction zone are more important for ASIC function than those pointing away that contribute less to the interactions between the three

loops. Most likely the MTSET modification impairs the interactions between the three loops by steric hindrance. Thus, both disruption of interactions between loops in the finger-ball interaction zone by MTSET and forcing it into a conformation by Cd^{2+} impair channel function. This suggests that both the contact between the loops and some flexibility are required for efficient gating.

In the structural model of ASIC1, which represents the inactivated conformation of the channel, the central residues of the finger-ball interaction zone are, although close to the protein surface, oriented toward each other and mostly away from the protein surface. These residues seem not to be easily accessible, and calculation of the accessible surface by using the COOR SEARCH function implemented in the CHARMM c34 molecular mechanics software showed for the residues of the finger-ball interaction zone an accessible surface of less than 10% relative to the surface of the isolated amino acid, except for Asp-227 (34). However, Cys mutants of these residues were efficiently modified by both small and large sulfhydryl reagents. In our experiments MTS reagents were normally applied to the channel in its closed state. When the exposure to MTSET was done under pH conditions that induce hASIC1a inactivation, the effect of MTSET on ASIC function was reduced in the mutants N96C, G162C, and H163C, indicating that the accessibility or the reactivity of these engineered Cys residues is different between the closed and inactivated channels. The most likely explanation for this observation is that inactivation induces conformational changes in the loops 1 and/or 2 of the finger-ball interaction zone. Exposure of N96C to a position different from that in the crystal structure may lead to its much higher reactivity to MTSET as compared with the other engineered Cys residues in this zone. The changed position of loop 1 (containing N96C) in the closed conformational state may be the cause of the increased accessibility for MTSET of G162C and H163C of loop 2 in the closed state as compared with the inactivated state. An orientation of N96C in the closed state that is different from the one in the structural model is also consistent with the observation that N96C binds Cd^{2+} without a contribution of His-163 (Fig. 3*B*). Even in the closed state, conformation N96C may not be completely exposed to the protein surface, as the observed molar reaction rate was still ~60 times lower than observed on an exposed engineered residue in the cystic fibrosis transmembrane regulator pore (31) or more than 1000-fold lower than measured on an engineered Cys residue in the voltage-gated Na^+ channel inactivation gate (32). Our observation of a conformational change is in contrast with the prediction from normal mode analysis that this domain would move as a whole during channel activation (14). Experiments with environment-sensitive dyes or with fluorescence resonance energy transfer may provide information on possible conformational changes of this zone during activation and on the direction of the observed changes (13).

In conclusion, the finger domain has previously been shown to be important for ASIC pH dependence. The main contact between the finger and the rest of the protein is in the finger-ball interaction zone. We show here that this zone is critical for ASIC expression and function and undergoes conformational changes during inactivation.

Acknowledgments—We thank Laurent Schild, Aurélien Boillat, Maxime Blanchard, Miguel van Bemmelen, and Delphine Huser for their comments on a previous version of the manuscript and for many discussions. We greatly appreciate the help of Justyna Iwaszkiewicz for the homology modeling of human ASIC1a. We thank John Wemmie for providing the ASIC1 antibodies and David Corey for providing the human ASIC1a clone.

REFERENCES

1. Krishtal, O. (2003) *Trends Neurosci.* **26,** 477–483
2. Wemmie, J. A., Price, M. P., and Welsh, M. J. (2006) *Trends Neurosci.* **29,** 578–586
3. Kellenberger, S., and Schild, L. (2002) *Physiol. Rev.* **82,** 735–767
4. Gonzales, E. B., Kawate, T., and Gouaux, E. (2009) *Nature* **460,** 599–604
5. Jasti, J., Furukawa, H., Gonzales, E. B., and Gouaux, E. (2007) *Nature* **449,** 316–323
6. Sutherland, S. P., Benson, C. J., Adelman, J. P., and McCleskey, E. W. (2001) *Proc. Natl. Acad. Sci. U.S.A.* **98,** 711–716
7. Sluka, K. A., Price, M. P., Breese, N. M., Stucky, C. L., Wemmie, J. A., and Welsh, M. J. (2003) *Pain* **106,** 229–239
8. Deval, E., Noël, J., Lay, N., Alloui, A., Diochot, S., Friend, V., Jodar, M., Lazdunski, M., and Lingueglia, E. (2008) *EMBO J.* **27,** 3047–3055
9. Mogil, J. S., Breese, N. M., Witty, M. F., Ritchie, J., Rainville, M. L., Ase, A., Abbadi, N., Stucky, C. L., and Séguéla, P. (2005) *J. Neurosci.* **25,** 9893–9901
10. Wemmie, J. A., Chen, J., Askwith, C. C., Hruska-Hageman, A. M., Price, M. P., Nolan, B. C., Yoder, P. G., Lamani, E., Hoshi, T., Freeman, J. H., Jr., and Welsh, M. J. (2002) *Neuron* **34,** 463–477
11. Wemmie, J. A., Askwith, C. C., Lamani, E., Cassell, M. D., Freeman, J. H., Jr., and Welsh, M. J. (2003) *J. Neurosci.* **23,** 5496–5502
12. Xiong, Z. G., Zhu, X. M., Chu, X. P., Minami, M., Hey, J., Wei, W. L., MacDonald, J. F., Wemmie, J. A., Price, M. P., Welsh, M. J., and Simon, R. P. (2004) *Cell* **118,** 687–698
13. Passero, C. J., Okumura, S., and Carattino, M. D. (2009) *J. Biol. Chem.* **284,** 36473–36481
14. Yang, H., Yu, Y., Li, W. G., Yu, F., Cao, H., Xu, T. L., and Jiang, H. (2009) *PLoS Biol.* **7,** e1000151
15. Baron, A., Schaefer, L., Lingueglia, E., Champigny, G., and Lazdunski, M. (2001) *J. Biol. Chem.* **276,** 35361–35367
16. Paukert, M., Chen, X., Polleichtner, G., Schindelin, H., and Gründer, S. (2008) *J. Biol. Chem.* **283,** 572–581
17. Bässler, E. L., Ngo-Anh, T. J., Geisler, H. S., Ruppersberg, J. P., and Gründer, S. (2001) *J. Biol. Chem.* **276,** 33782–33787
18. Vukicevic, M., Weder, G., Boillat, A., Boesch, A., and Kellenberger, S. (2006) *J. Biol. Chem.* **281,** 714–722
19. Martí-Renom, M. A., Stuart, A. C., Fiser, A., Sánchez, R., Melo, F., and Sali, A. (2000) *Annu. Rev. Biophys. Biomol. Struct.* **29,** 291–325
20. Shen, M. Y., and Sali, A. (2006) *Protein Sci.* **15,** 2507–2524
21. Melo, F., and Feytmans, E. (1997) *J. Mol. Biol.* **267,** 207–222
22. Laskowski, R. A., MacArthur, M. W., Moss, D. S., and Thornton, J. M. (1993) *J. Appl. Crystallogr.* **26,** 283–291
23. Kadurin, I., Golubovic, A., Leisle, L., Schindelin, H., and Gründer, S. (2008) *Biochem. J.* **412,** 469–475
24. Babini, E., Paukert, M., Geisler, H. S., and Grunder, S. (2002) *J. Biol. Chem.* **277,** 41597–41603
25. Coscoy, S., de Weille, J. R., Lingueglia, E., and Lazdunski, M. (1999) *J. Biol. Chem.* **274,** 10129–10132
26. Kellenberger, S., Gautschi, I., and Schild, L. (1999) *Proc. Natl. Acad. Sci. U.S.A.* **96,** 4170–4175
27. Zhang, P., and Canessa, C. M. (2002) *J. Gen. Physiol.* **120,** 553–566
28. Salinas, M., Rash, L. D., Baron, A., Lambeau, G., Escoubas, P., and Lazdun-

ski, M. (2006) *J. Physiol.* **570,** 339–354
29. Li, T., Yang, Y., and Canessa, C. M. (2009) *J. Biol. Chem.* **284,** 4689–4694
30. Heinz, U., Bauer, R., Wommer, S., Meyer-Klaucke, W., Papamichaels, C., Bateson, J., and Adolph, H. W. (2003) *J. Biol. Chem.* **278,** 20659–20666
31. Zhang, Z. R., Song, B., and McCarty, N. A. (2005) *J. Biol. Chem.* **280,** 41997–42003
32. Kellenberger, S., Scheuer, T., and Catterall, W. A. (1996) *J. Biol. Chem.* **271,** 30971–30979
33. Pettersen, E. F., Goddard, T. D., Huang, C. C., Couch, G. S., Greenblatt, D. M., Meng, E. C., and Ferrin, T. E. (2004) *J. Comput. Chem.* **25,** 1605–1612
34. Liechti, L. A., Berneche, S., Bargeton, B., Iwaszkiewicz, J., Roy, S., Michielin, O., and Kellenberger, S. (March 18, 2010) *J. Biol. Chem.* 10.1074/jbc.M109.092015

SUPPLEMENTAL MATERIAL FOR

THE CONTACT REGION BETWEEN THREE DOMAINS OF THE EXTRACELLULAR LOOP OF ASIC1A IS CRITICAL FOR CHANNEL FUNCTION

Benoîte Bargeton and Stephan Kellenberger
From the Department of Pharmacology and Toxicology, University of Lausanne, CH-1005 Lausanne, Switzerland

SUPPLEMENTAL EXPERIMENTAL PROCEDURES

Cell surface protein biotinylation and western blot analysis – The experiments described in Fig. S2 were carried out exactly as described in "*Experimental procedures*" except for the number of oocytes per condition which was 40.

Electrophysiological analysis of MTSET kinetics experiments – The stimulation solution of pH 5.5 was applied once every minute during 5 s. Between acidic stimulations, the recording chamber was perfused with the conditioning solution at pH 7.4, which was changed after 4-5 acidic stimulations to one containing MTSET at a concentration that allowed resolution of the kinetics of current decrease, as indicated for each of the three mutants shown in Fig. S3B. Immediately before each acidic stimulation the conditioning solution with MTSET was changed for 5 s to one containing no MTSET. Kaleidagraph (Synergy software) was used to fit the kinetics of the current decrease of the normalized data, by using the equation: $I = a + (1- a)\cdot\exp^{-kt}$, where I is the peak current amplitude normalized to that before MTSET addition, a, is the fraction of normalized current that is not inhibited by MTSET, k is the rate constant in min^{-1} and t is the time after start of MTSET exposure in min.

SUPPLEMENTAL FIGURE LEGENDS

Figure S1. Structure of the finger-ball interaction zone in ASIC1a in Stereo view. A, Structure of hASIC1a established by homology modeling based on cASIC1 (PDB ID 2QTS). One of the three ASIC subunits is shown in color, identifying different parts of ASIC subunits (red: transmembrane segments, yellow: palm, orange: β-ball, green: thumb, purple: finger, turquoise: knuckle. B, View of the finger-ball interaction zone with loop 1 in black, loop 2 in grey and loop 3 in brown. The side chains of the residues mutated in this study are represented as "ball-and-stick" (Category I residues, see text) and as "stick" (Category II residues). Hydrogen bonds predicted in Chimera (1) are indicated as blue solid lines.

Figure S2. ASIC protein and current expression. A, Representative Western blots of the cell surface expression of ASIC1a wt and ASIC1a H163C fused or not to UTR of *Xenopus* β-globin (see *Experimental Procedures*) as indicated. Cell-surface proteins were isolated by biotinylation, as described under "*Experimental Procedures*" from 40 ASIC1a-expressing oocytes 1 day after injection of 10 ng of cRNA. ASIC1a (~70 kDa) was visualized by a specific antibody (MTY19, (2)) that recognizes a C-terminal epitope of hASIC1. Representative blots of the unbound and the bound fraction from one out of 3 similar experiments per channel type are shown. The bands in the unbound fraction of non-injected oocytes are from a contamination of neighboring lanes. **B**, Peak current amplitude of ASIC1a wt and ASIC1a H163C fused or not to UTR of *Xenopus* β-globin induced by acidification to pH 4.5 at a holding potential of -60 mV, 1-2 days after injection of 10 ng (wt) or 10-50 ng cRNA per oocyte (mutants; n = 15-86 per condition, presented as mean ± SEM). *, different, $p < 0.05$ (ANOVA and Dunnet post hoc test). The pH50 of activation of ASIC1a wt (6.1 ± 0.0, n=3) and H163C (6.0 ± 0.0, n=4) are not modified by the UTR *Xenopus* β-globin fusion (6.1 ± 0.0, n=3 and 6.0 ± 0.0, n=4 for ASIC wt and H163C, respectively; data not shown).

Figure S3. Kinetics of peak current inhibition of selected ASIC1a mutants by extracellular MTSET. A, Representative current traces of oocytes expressing ASIC1a Q225C obtained by 5-s acidification to the indicated pH values at a holding potential of -60 mV, before and during incubation with 0.15 mM MTSET. **B**, pH 5.5-induced peak current amplitude, normalized to the amplitude before application of the reagent, shown before and during exposure to MTSET for the ASIC1a mutants N96C (▼, MTSET 0.01mM), H163C (●, MTSET 0.25 mM) and Q225C (▲, MTSET 0.15 mM) (n = 4-6). Data are presented as mean ± SEM. The lines represent fits to single exponential (see *Supplemental Experimental Procedures*) yielding a rate constant k (min^{-1}) of current decrease. **C**, Rate constant (k, min^{-1} M^{-1}) of MTSET inhibition of peak currents of mutant channels of category I, calculated from the rate of current decrease (in min^{-1}) divided by the concentration of MTSET used (in M), mean ± SEM . *, Kinetic constant different from other mutant channels, $p < 0.05$ (ANOVA and Dunnet post hoc test).

Figure S4. Time constant of open channel inactivation of ASIC1a wt and mutants. ASIC currents were induced by acidification to pH 6.0 or 4.5 before and after a 5-min incubation with 1 mM MTSET and measured at a holding potential of -60 mV. The time course of open-channel inactivation of the traces was fitted to a single exponential by using Clampfit (Molecular Devices), yielding the time constants presented. *, different from wt (same condition), $p < 0.05$ (ANOVA and Dunnet post hoc test).

REFERENCES FOR SUPPLEMENTAL DATA

1. Pettersen, E. F., Goddard, T. D., Huang, C. C., Couch, G. S., Greenblatt, D. M., Meng, E. C., and Ferrin, T. E. (2004) *J Comput Chem* **25**, 1605-1612
2. Wemmie, J. A., Askwith, C. C., Lamani, E., Cassell, M. D., Freeman, J. H., and Welsh, M. J. (2003) *J. Neurosci.* **23**, 5496-5502

A

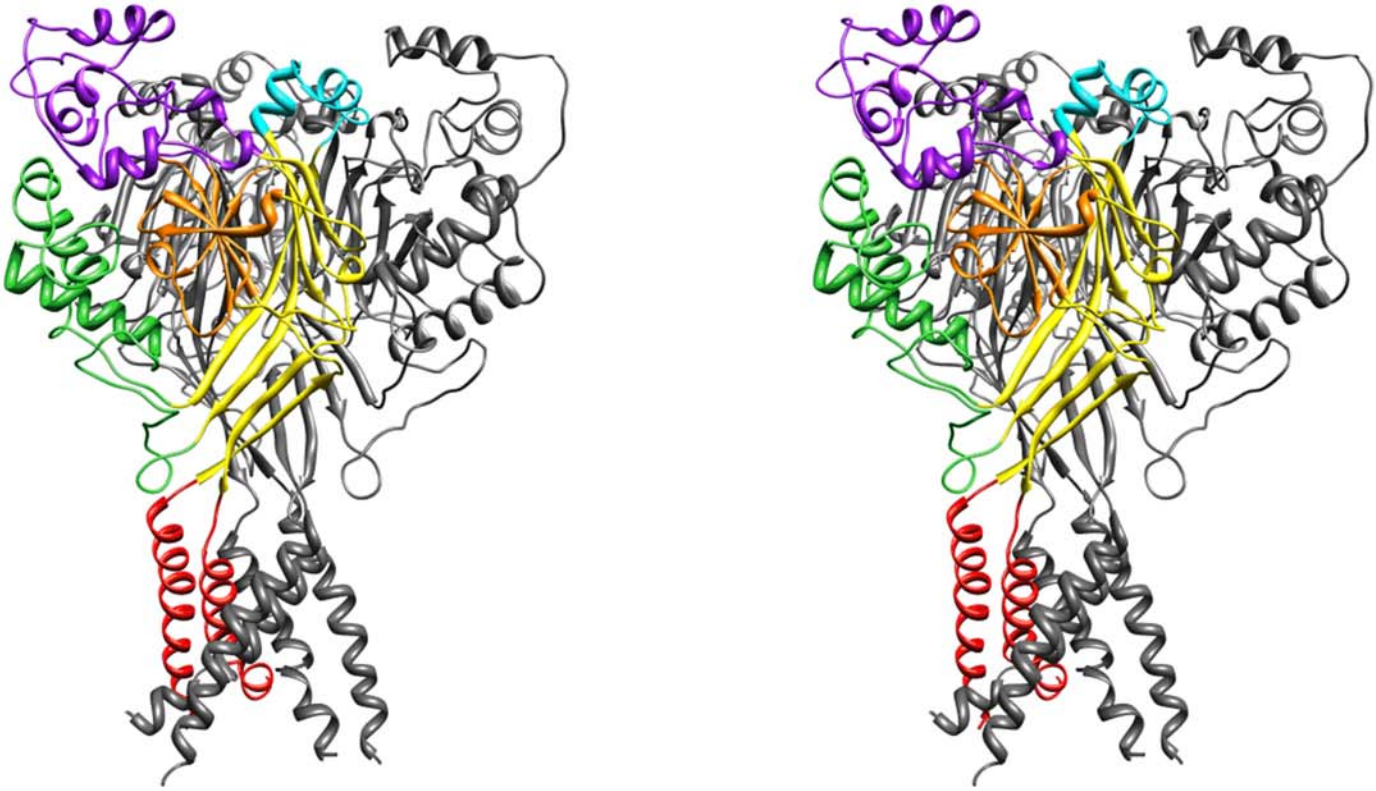

B

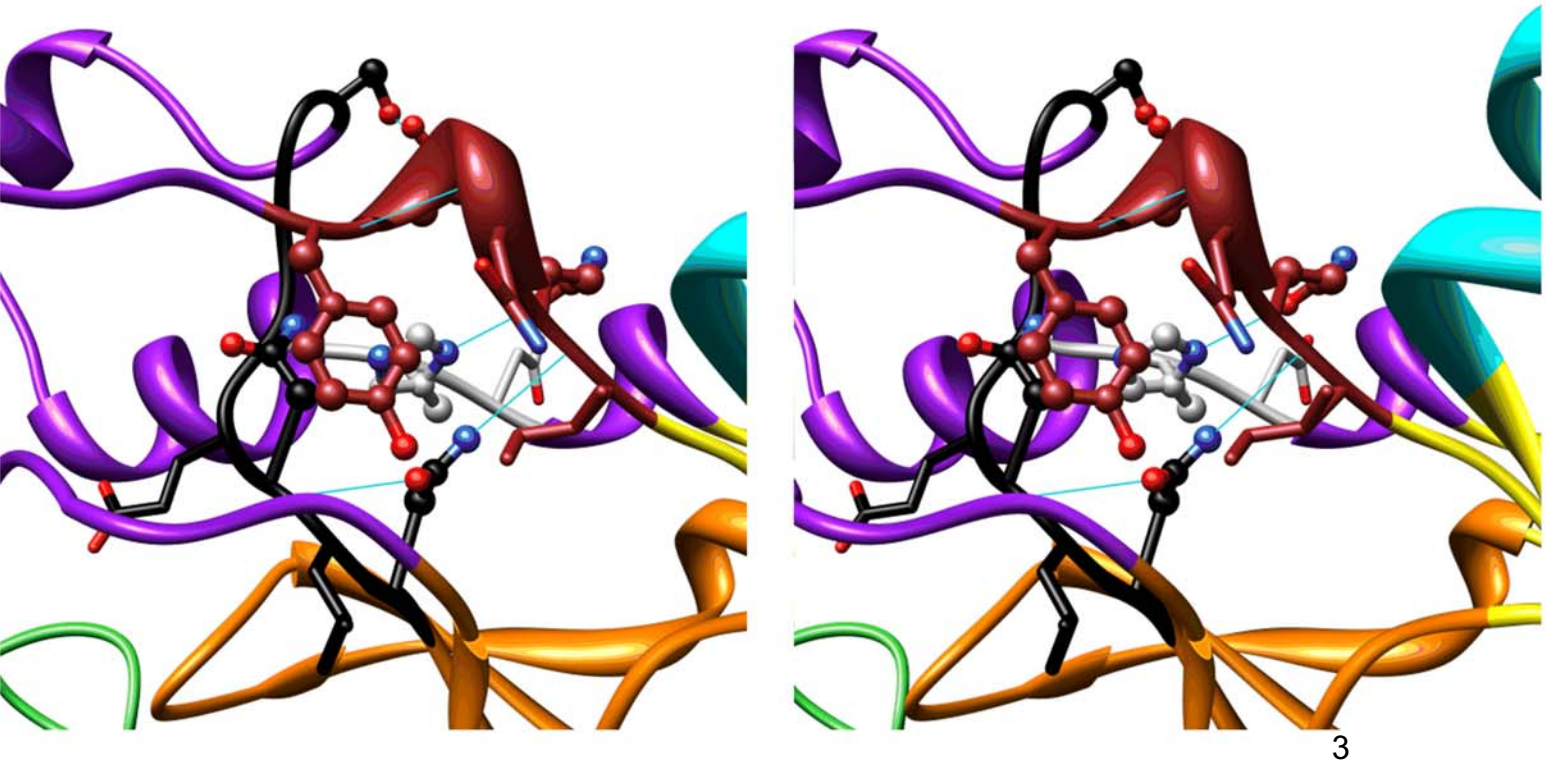

Figure S1

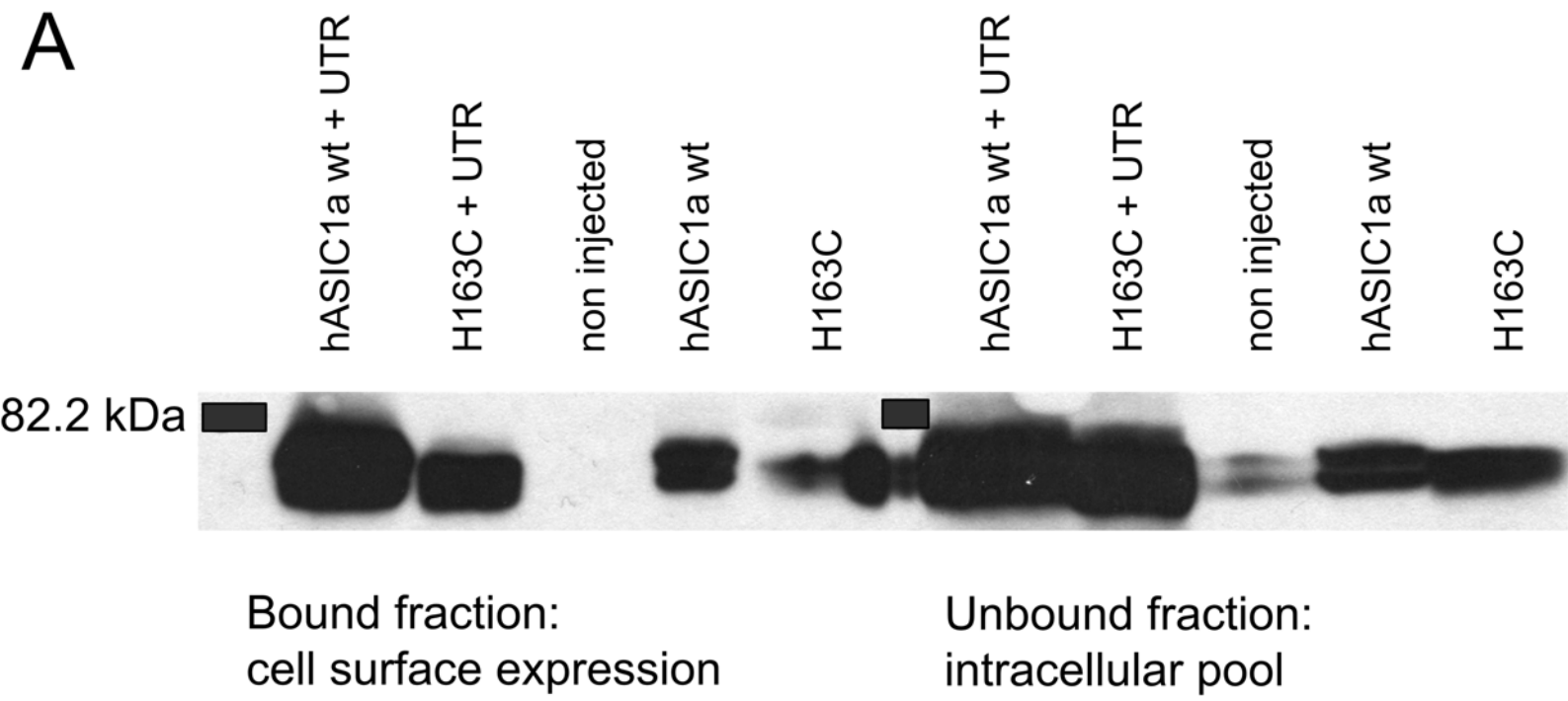
A
hASIC1a wt + UTR
H163C + UTR
non injected
hASIC1a wt
H163C
hASIC1a wt + UTR
H163C + UTR
non injected
hASIC1a wt
H163C
82.2 kDa
Bound fraction:
cell surface expression
Unbound fraction:
intracellular pool

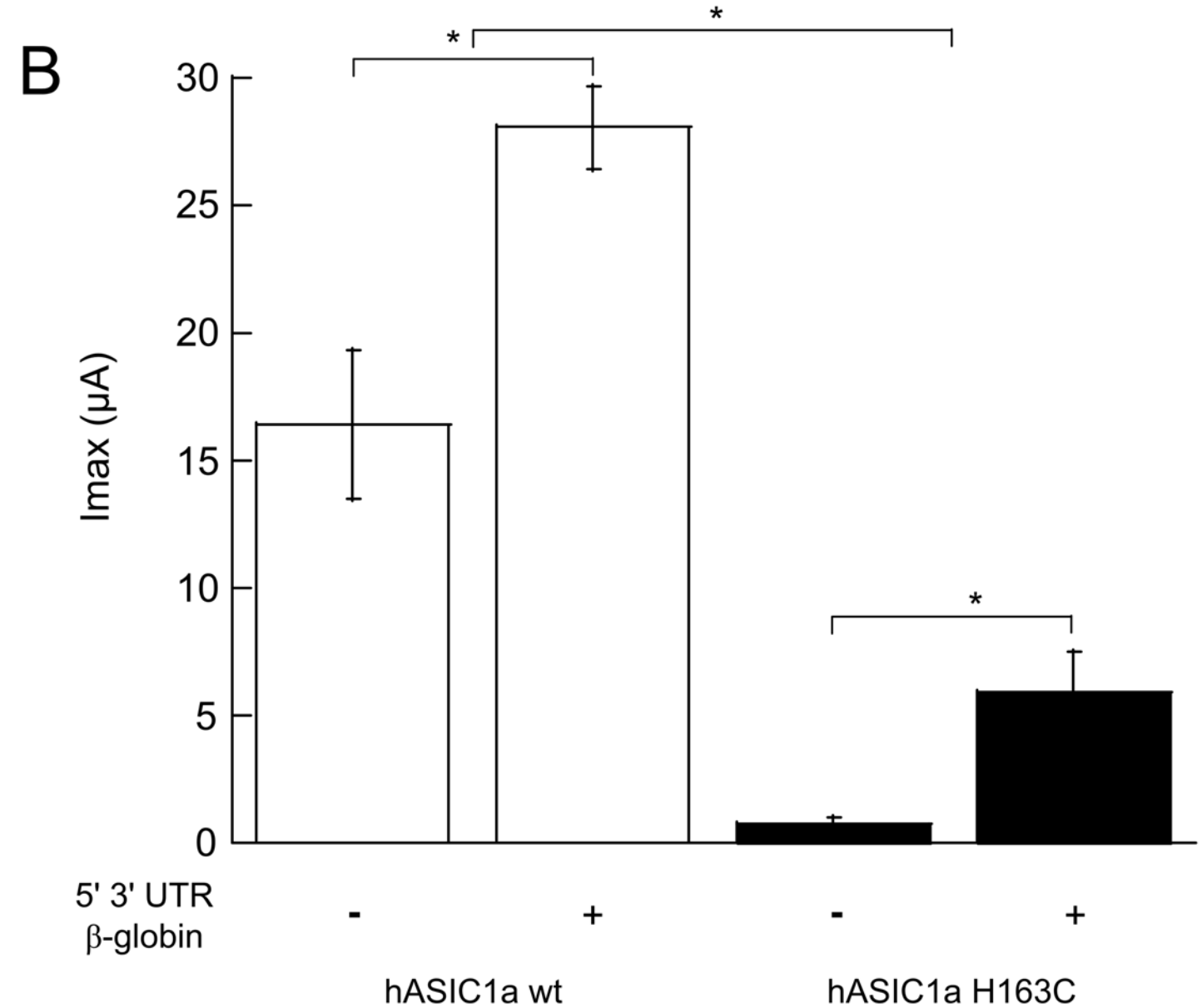
B
*
*
*
30
25
20
15
10
5
0
Imax (μA)
5' 3' UTR
β-globin
-
+
-
+
hASIC1a wt
hASIC1a H163C

Figure S2

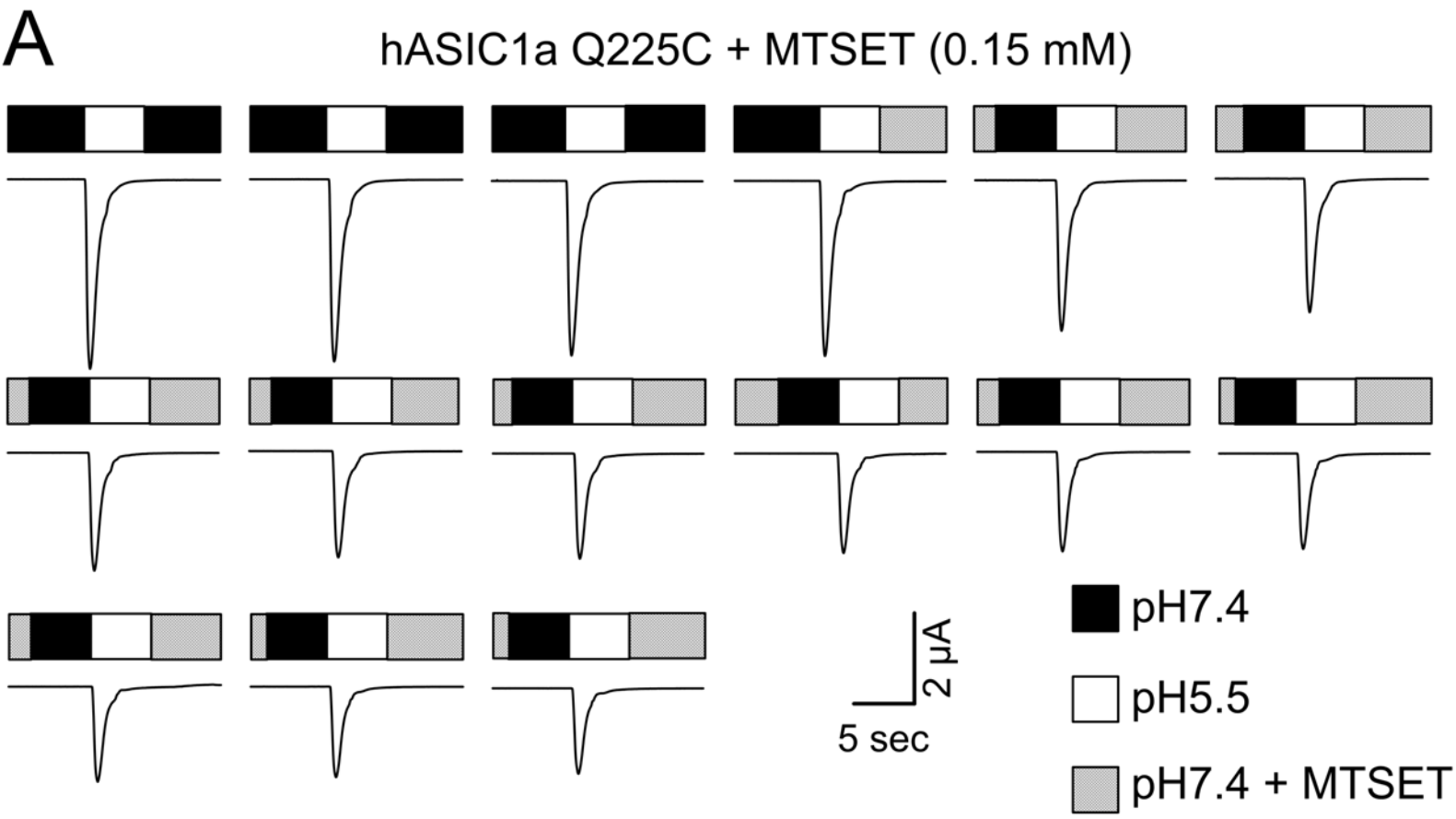

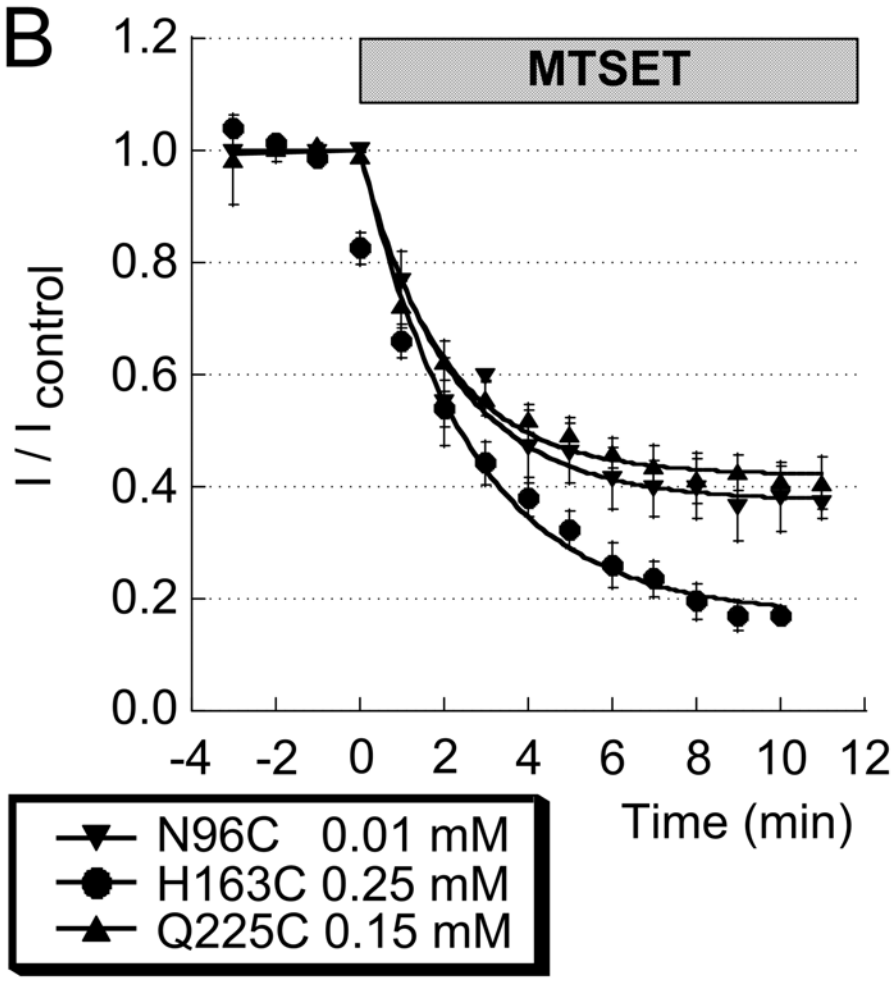

C Rate constant of MTSET-induced current decrease

hA1a	k ($M^{-1}min^{-1}$)
N94C	2696 ± 1091
N96C*	26130 ± 4869
S101C	1677 ± 528
G162C	1739± 591
H163C	1540 ± 154
Q225C	3055 ± 383
E228C	6861 ± 1175

Figure S3

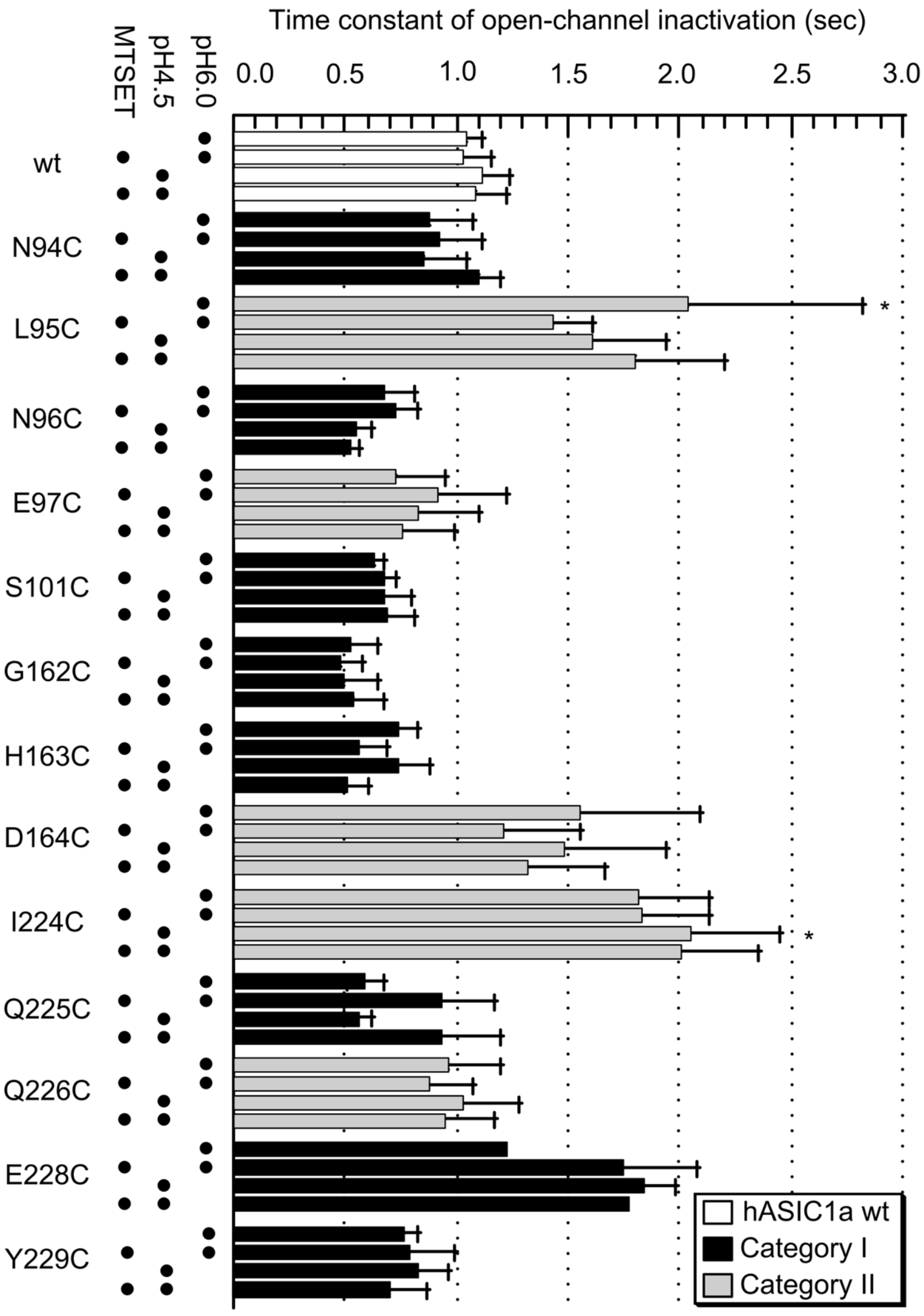
Time constant of open-channel inactivation (sec)
0.0
0.5
1.0
1.5
2.0
2.5
3.0
MTSET
pH4.5
pH6.0
wt
N94C
L95C
N96C
E97C
S101C
G162C
H163C
D164C
I224C
Q225C
Q226C
E228C
Y229C
*
*
hASIC1a wt
Category I
Category II

Figure S4